



Escola Tècnica Superior d'Enginyeries
Industrial i Aeronàutica de Terrassa

UNIVERSITAT POLITÈCNICA DE CATALUNYA

**STUDY OF THE MECHANICAL RESPONSE
OF THE LTP'S TEST MASSES
DUE TO THE ACTION OF CONTROL HEATERS
IN LISA PATHFINDER**

- APPENDICES -

PROJECTE FINAL DE CARRERA D'ENGINYERIA AERONÀUTICA

AUTHOR: FERRAN GIBERT GUTIÉRREZ
TUTORS: ALBERTO LOBO AND EDWARD CHESTER
SCHOOL TUTOR: ELENA FANTINO

Terrassa, January 2011

Contents

List of Figures	iii
List of Tables	iv
A Thermal model notation	1
A.1 Electrode nodes notation	1
A.2 EH thermal items connectivities	4
B View factors computation	5
B.1 Frontal surfaces	7
B.2 Perpendicular surfaces	9
C Thermistor's heat radiation losses	11
D Control loop	13
E Budget	16
F Related publications	18

List of Figures

A.1	Electrode nodes notation for the X face of the EHs. Red circles represent the different EH heaters and green circles stand for the temperature sensors location.	2
A.2	Electrode nodes notation for the Y and Z faces of the EHs.	3
B.1	Parallel surfaces scheme [2].	6
B.2	Perpendicular surfaces scheme [2].	6
B.3	View factor 1.	7
B.4	View factor 2.	7
B.5	View factor 3.	8
B.6	View factor 4.	8
B.7	View factor 5.	8
B.8	View factor 6.	9
B.9	View factor 1.	10
B.10	View factor 2.	10
C.1	NTC thermistor photo [3].	12

D.1	Diagram of the control loop.	14
-----	--------------------------------------	----

List of Tables

A.1 Thermal nodes of each DDS item from the EH and the nodes where they are attached.	4
B.1 View factors values for parallel surfaces	9
B.2 View factors values for perpendicular surfaces.	10
E.1 Software costs.	16
E.2 Hardware costs.	16
E.3 Working hours cost.	17
E.4 Total costs.	17

Appendix A

Thermal model notation

The LPF thermal model is a FEM model with more than 20,000 thermal nodes, so a clear notation is required in order to easily identify each node without ambiguity. Although a detailed explanation of the complete notation can be found at [1], a selection of the nodes appearing in the algorithm is presented.

Specifically, this appendix presents the notation of next parts:

1. Electrode nodes notation
2. External EH nodes notation
3. EH thermal items connectivities

A.1 Electrode nodes notation

Figures A.1 and A.2 present the notation of each thermal node representing the different electrodes from the EH.

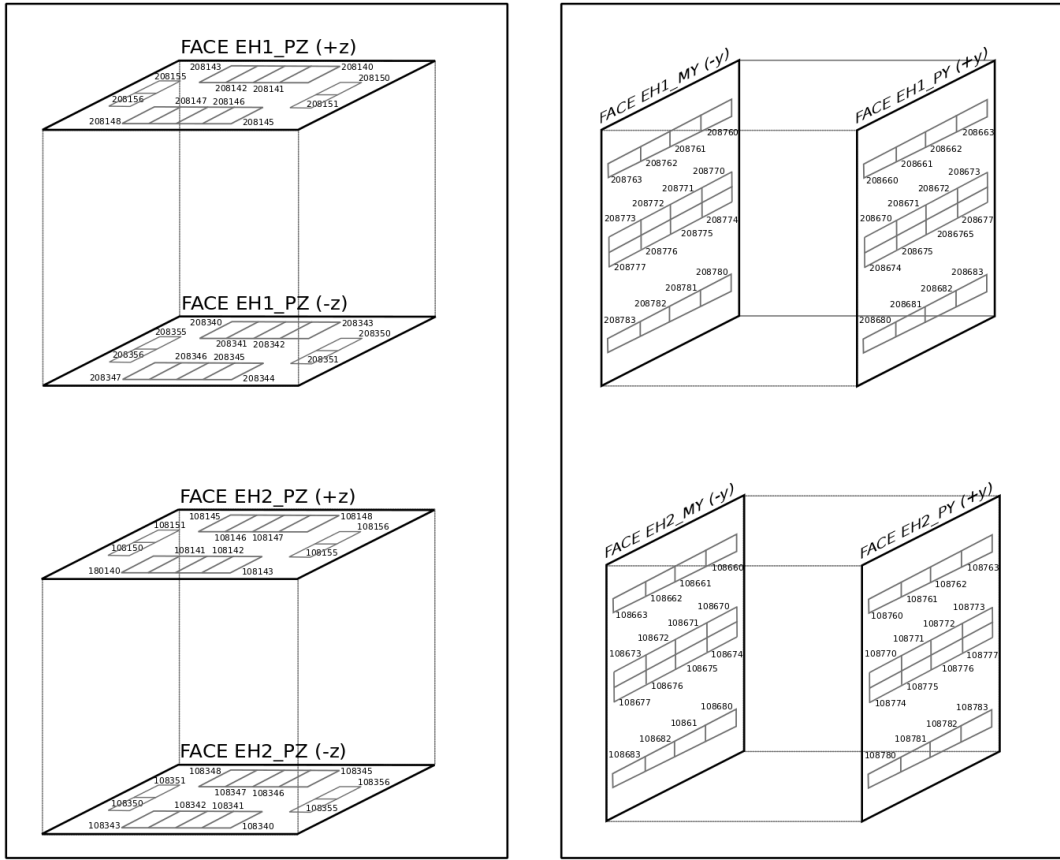


Figure A.2: Electrode nodes notation for the Y and Z faces of the EHs.

A.2 EH thermal items connectivities

Tables A.1 shows the EH thermal nodes where the different EH items are linked, as extracted from [1].

DDS id	Node in the model	Node where it is attached
TS1	716008	208506
TS2	716007	208509
TS3	716006	208405
TS4	716005	208410
TS5	716002	108509
TS6	716001	108506
TS7	716004	108410
TS8	716003	108405
H1-1	713007	208510
H1-2	713008	208505
H2-1	713005	208409
H2-2	713006	208406
H3-1	713004	108409
H3-2	713003	108406
H4-1	713002	108510
H4-2	713001	108505

Table A.1: Thermal nodes of each DDS item from the EH and the nodes where they are attached.

Appendix B

View factors computation

The different view factors appearing along the document are recopied and calculated in this Appendix.

There are two type of pairs of visible surfaces in the document depending on their relative position: *parallel* surfaces and *perpendicular* surfaces. As all the surfaces appearing along the algorithm are rectangular, the following expressions from [2] have been applied.

- For parallel surfaces as ones in Figure B.1:

$$F_{1-2} = \frac{1}{(x_2 - x_1)(y_2 - y_1)} \sum_{l=1}^2 \sum_{k=1}^2 \sum_{j=1}^2 \sum_{i=1}^2 (-1)^{(i+j+k+l)} G(x_i, y_j, \eta_k, \xi_l) \quad (\text{B.1})$$

where

$$\begin{aligned} G = & \frac{1}{2\pi} \left((y - \eta) [(x - \xi)^2 + z^2]^{1/2} \tan^{-1} \left\{ \frac{y - \eta}{[(x - \xi)^2 + z^2]^{1/2}} \right\} \right. \\ & + (x - \xi) [(y - \eta)^2 + z^2]^{1/2} \tan^{-1} \left\{ \frac{x - \xi}{[(y - \eta)^2 + z^2]^{1/2}} \right\} \\ & \left. - \frac{z^2}{2} \ln [(x - \xi)^2 + (y - \eta)^2 + z^2] \right) \quad (\text{B.2}) \end{aligned}$$

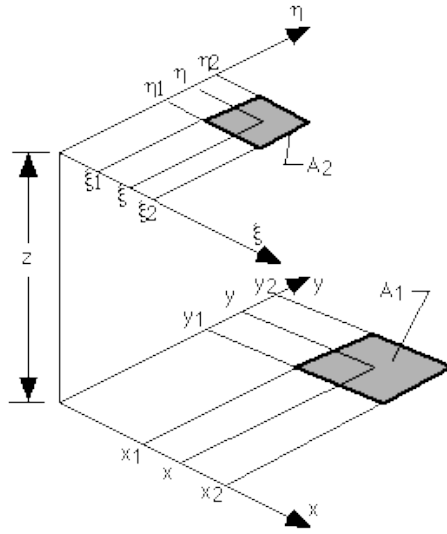


Figure B.1: Parallel surfaces scheme [2].

- For perpendicular surfaces as ones in Figure B.2:

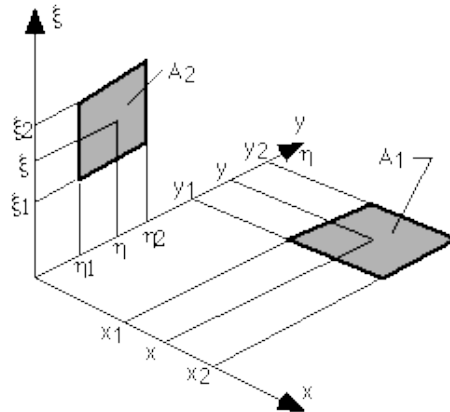


Figure B.2: Perpendicular surfaces scheme [2].

$$F_{1-2} = \frac{1}{(x_2 - x_1)(y_2 - y_1)} \sum_{l=1}^2 \sum_{k=1}^2 \sum_{j=1}^2 \sum_{i=1}^2 \left[(-1)^{(i+j+k+l)} G((x_i, y_j, \eta_k, \xi_l)) \right] \quad (\text{B.3})$$

with

$$G = \frac{1}{2\pi} \left\{ (y-\eta)(x^2+\xi^2)^{1/2} \tan^{-1}(K) - \frac{1}{4} \left[(x^2+\xi^2) \ln(1+K^2) - (y-\eta)^2 \ln \left(1 + \frac{1}{K^2} \right) \right] \right\} \quad (\text{B.4})$$

$$K = \frac{(y-\eta)}{(x^2+\xi^2)^{1/2}} \quad (\text{B.5})$$

B.1 Frontal surfaces

Six different view factors have been identified, depending on the possible combinations of parallel facets in the algorithm .

1. View factor from a whole EH inner face to a whole TM face, as shown in Figure B.3.

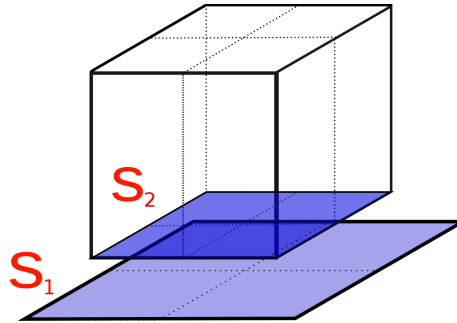


Figure B.3: View factor 1.

2. View factor from a squared EH facet to a TM *frontal* facet, as shown in Figure B.4.

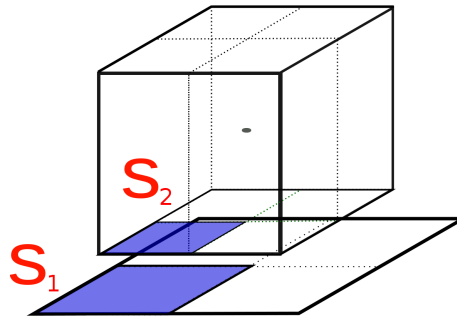


Figure B.4: View factor 2.

3. View factor from a squared EH facet to a *near* TM frontal facet, as shown in Figure B.5.

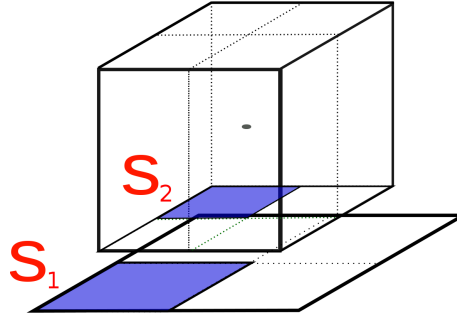


Figure B.5: View factor 3.

4. View factor from a squared EH facet to a *crossed* TM frontal facet, as shown in Figure B.6.

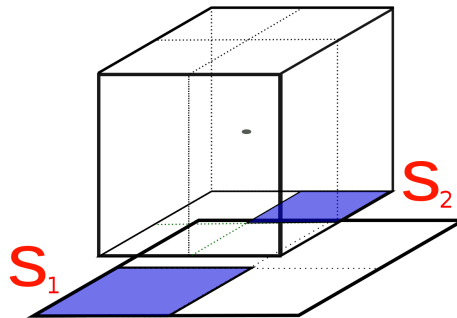


Figure B.6: View factor 4.

5. View factor from a rectangular EH facet to a *frontal* rectangular TM facet, as shown in Figure B.7.

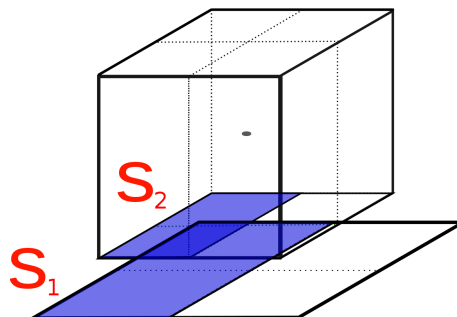


Figure B.7: View factor 5.

- View factor from a rectangular EH facet to a *crossed* TM facet, as shown in Figure B.8.

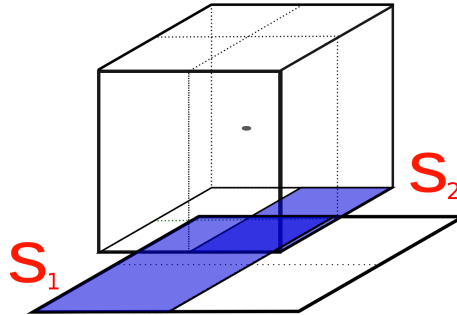


Figure B.8: View factor 6.

These view factors have been calculated considering a nominal distance EH-TM of 4mm and an inner EH side of 0.054mm. The TM side is 0.046mm. Table B.1 shows the values obtained, applying Equation B.1.

View factor	Value
1	0.6831
2	0.5861
3	0.0454
4	0.0062
5	0.6315
6	0.0516

Table B.1: View factors values for parallel surfaces

B.2 Perpendicular surfaces

Two cases have been considered for perpendicular surfaces.

- View factor from a whole EH inner square facet to an adjacent TM rectangular facet, as shown in Figure B.9.

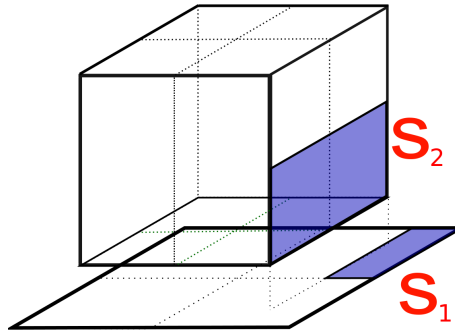


Figure B.9: View factor 1.

2. View factor from a whole EH inner square facet to a *not-adjacent* TM rectangular facet, as shown in Figure B.10.

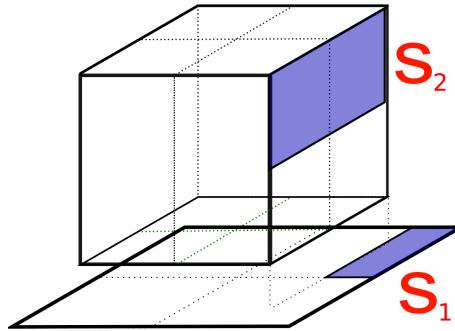


Figure B.10: View factor 2.

In both cases, only the fraction of surface presenting visibility towards the other has been initially considered for the calculus applying Equation B.3. However, the fraction that it represents is computed in the final values presented in Table B.2.

View factor	Value from Figure	Fraction area	Real facet-to-facet view factor
7	0.1342	0.087	0.0117
8	0.0093	0.087	0.00081

Table B.2: View factors values for perpendicular surfaces.

Due to the low values of the view factors from Table B.2, they have not been considered in the algorithm. Therefore, only view factors from parallel surfaces presenting direct visibility have been considered in the model.

Appendix C

Thermistor's heat radiation losses

One of the strongest hypotheses considered in this report is that heater's heat lost by radiation is negligible in front of the heat flux that is injected into the EH. In order to justify this, some numbers are presented in this Appendix.

First, we assume a heater's exposed area of about $A \approx (0.01)^2 \text{ m}^2$ and an emissivity coefficient of $\epsilon_{heater} \approx 0.9$, that corresponds to the black epoxy layer covering the heaters, as well as to the emissivity of the EH material, therefore $\epsilon_{EH} \sim \epsilon_{heater} \sim \epsilon$.

Considering the nominal initial temperature in the EH environment to be of approximately $T_0 = 293\text{K}$, and a maximum increase of temperature -a conservative one- in the heater's surface of $\Delta T = 1\text{K}$ respect to the rest of the environment, the total amount of radiated power is defined with Equation C.1.

$$\dot{Q}_{RAD} = \epsilon A \sigma (T_{heater}^4 - T_0^4) = \epsilon A \sigma \left((T_0 + \Delta T)^4 - T_0^4 \right) \quad \text{W} \quad (\text{C.1})$$

where $\sigma = 5.6704 \times 10^{-8} \text{ Wm}^{-2}\text{K}^{-4}$ is the Stefan-Boltzmann constant. Replacing with the values, it is obtained

$$\dot{Q}_{RAD} = 5.16 \times 10^{-4} \approx 0.5 \text{ mW} \quad (\text{C.2})$$

This 0.5mW are obtained when $\sim 40\text{mW}$ are injected to a heater, causing $\Delta T = 1\text{K}$.

Therefore, the radiated heat represents

$$\frac{0.5\text{mW}}{40\text{mW}} \times 100 = 1.25\% \quad (\text{C.3})$$

of total heat injected.

So, the hypothesis of neglecting the radiated heat can be applied if an error of about 1.25% is acceptable.



Figure C.1: NTC thermistor photo [3].

Appendix D

Control loop

The ultimate goal of the thermal effects simulation is to add them in the simulator of the LTP control loop of the whole LPF simulator, so as to see if under their execution both the LTP and the spacecraft behave properly.

This simulator of the LTP control loop takes as inputs mission telecommands and returns as outputs GRS and IFO readouts. It is a state space model (SSM) of the whole spacecraft that collects all the different sensors, actuators and controllers of the LTP and simulates its behaviour and their interactions while performing. Consequently, it gathers the different effects, noise sources and transfer functions established between the different components, so the global behaviour of the satellite under its nominal operative conditions can be simulated. It is being developed by the LTPDA group, based in Hannover, which is programming it in MATLAB, as well as developing a wide Toolbox aimed to unify the most common functions and classes to be used in the different data analysis of the mission.

The LTP control loop uses the set of sensors readings and drives the actuators to keep the masses centred in their relative position with in the spacecraft. As has been described in Section 2.3.2, the LTP IFO provides different readouts:

- **x1**: Displacement of drag-free mass, *TM1*, in relation to the spacecraft.

- **x12**: Displacement of drag-free mass, *TM1*, in relation to *TM2*.

Each one is used in the control loop as a sensor readout, and then their measurements are introduced in the loop controller, the so called *Drag-Free and Attitude Control System* (DFACS) controller. Figure D.1 shows a scheme of the loop.

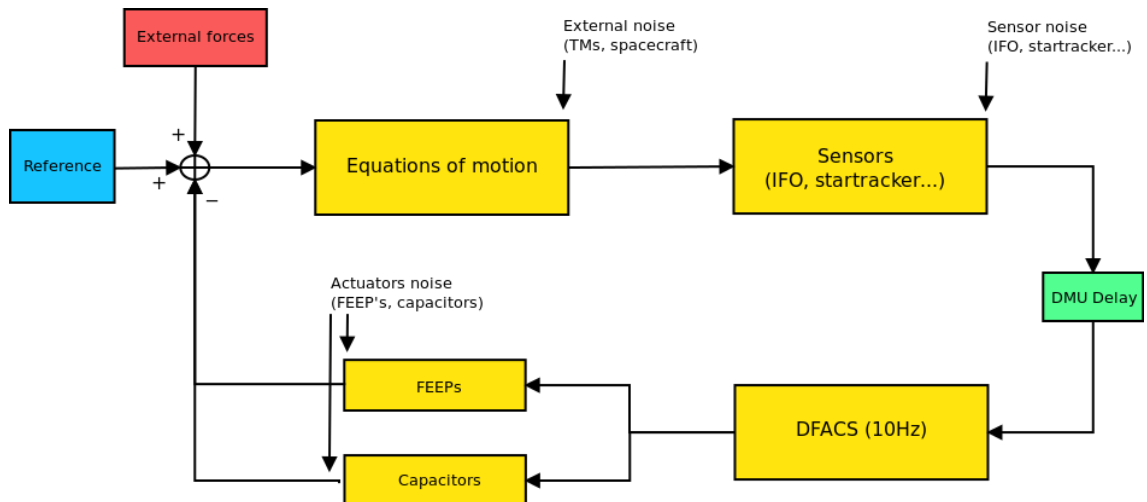


Figure D.1: Diagram of the control loop.

There are two main controllers in the loop:

- The *Drag-free controller*. This controller forces the spacecraft to follow the geodesic trajectory of *TM1*. Therefore, it must compensate the different external disturbances that affect the spacecraft, i.e. solar radiation and other external noises. It does so by means of micro-newton thrusters, that work as actuators in the loop. This controller reads the **x1** signal and sends suitable actuation commands to the micro-thrusters.
- The *Low frequency suspension controller*. The drag-free controller cannot force the spacecraft to follow both TMs at the same time. Therefore *TM2* may be drifting away from its centred position relative to the spacecraft, and this has to be compensated for in order to keep the experiment alive. The low frequency suspension controller takes up this task: it acts on *TM2* so that it is driven back to the centred position very slowly, hence "low frequency" qualifier. This ensures that relative positions between the TMs are properly read by the IFO channel **x12**, as any corrections due to the forced drift of *TM2* will be only visible at frequencies

below the band of interest. The LF suspension controller acts by means of electric forces on TM2 generated in electrodes of EH2.

The thermal forces obtained in Chapter 7 are treated as *external forces* in the control loop (see Figure D.1, and the outputs are the time series of the IFO readouts showing how both TMs and the spacecraft move when thermal disturbances are applied on an EH.

The introduction of the thermal forces in the SSM will show the behaviour of the spacecraft when the test masses are acted on by means of thermal signals.

Appendix E

Budget

The cost of the development of this project is divided into different costs, presented in the following tables:

- Table E.1 presents the software costs.
- Table E.2 presents the hardware costs.
- Table E.3 the working time cost.

At the end, Table E.4 presents the total cost of the study.

Item	Annual license cost	Period applicable	Cost
ESATAN-TMS license	1230€	6 months	615€

Table E.1: Software costs.

Item	Unit cost	Amortization period	Period applicable	Cost
Laptop	813€	48 months	10 months	170€

Table E.2: Hardware costs.

Cost	Number of hours	Hour cost	Total
Total working hours	1450h	6€/h	8700€

Table E.3: Working hours cost.

Total HW and SW cost	785€
Total working hours cost	8700€
Total study cost	9485 €

Table E.4: Total costs.

The total cost of this study is of 9485€.

Appendix F

Related publications

As stated in the beginning of the document, the development of this work allowed the elaboration of a poster presentation in the 8th LISA Symposium that was held from June 28th to July 2nd, 2010, in the SLAC (*Stanford Linear Accelerator Center*), California, USA.

This has been submitted for publication in the proceedings volume of the Symposium in the *Journal of Physics: Conference Series*, in 2011. The manuscript is attached below.

Heater induced thermal effects on the LTP dynamics

F Gibert^{1,3}, A Lobo^{1,2}, M Diaz-Aguiló^{1,4}, I Mateos¹, M Nofrarias⁵, J Sanjuán⁶, A Conchillo^{1,2}, L Gesa^{1,2} and I Lloro^{1,2}

¹ Institut d'Estudis Espacials de Catalunya (IEEC), Barcelona, Spain

² Institut de Ciències de l'Espai (CSIC-IEEC), Barcelona, Spain

³ Escola Tècnica Superior d'Enginyeries Industrial i Aeronàutica de Terrassa (ETSEIAT), Universitat Politècnica de Catalunya (UPC), Terrassa, Spain

⁴ Escola Politècnica Superior de Castelldefels (EPSC), Universitat Politècnica de Catalunya (UPC), Castelldefels, Spain

⁵ Max-Planck-Institut für Gravitationsphysik, Albert Einstein Institut (AEI), Hannover, Germany

⁶ Department of Physics, University of Florida, Gainesville, FL, United States

E-mail: gibert@ieec.cat

Abstract. The STOC (Science and Technology Operations Centre) simulator of the LPF (LISA PathFinder) mission is intended to provide a validation tool for the mission operations tele-commanding chain, as well as for a deeper understanding of the underlying physical processes happening in the LTP (LISA Technology Package). Amongst the different physical effects that will appear onboard, temperature fluctuations in the Electrode Housing (EH) could generate disturbances on the interferometer (IFO) readouts, therefore they must be known and controlled. In this article we report on the latest progress in the analysis at IEEC of the LTP response to thermal signals injected by means of heaters. More specifically, we determine the transfer functions relating heat input signals to forces on the Test Masses (TMs) in the LTP frequency band, from 1 mHz to 30 mHz. A complete thermal model of the entire LPF spacecraft plus payload, elaborated and maintained at European Space Technology Center (ESTEC), was used to obtain temperature distributions in response to heat inputs at prescribed spots (heaters), which are later processed to calculate the associated dynamical effects on the Test Masses.

1. Introduction

Undesired temperature fluctuations around the TMs and in other points of LTP have been identified as disturbances that could alter IFO readouts. In order to keep them controlled, a set of experiments, gathered in the Experiment Master Plan (EMP), are planned to be conducted onboard LPF so the effects can be measured and later use the results to assess the weight of temperature noise in the global noise budget.

All this involves the necessity of modelling and simulating the different thermal effects. To achieve this goal, the STOC simulator of LPF, that is aimed to recreate the behavior of the spacecraft through its main operational phases, must include them.

In this article, we focus only on the consequences of thermal effects at EH due to the activation of the different Data and Diagnostics System (DDS) heaters following the plans from the EMP. Specifically, in the following a description of the process considered to determine forces acting on TMs is explained, as well as the simulations of the heat input in the system. In the last sections, results from the simulations are presented and discussed.

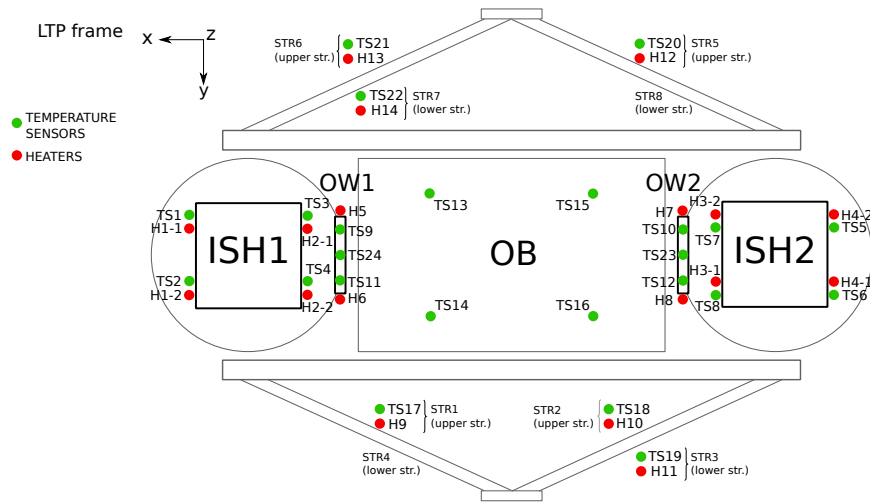


Figure 1. Figure caption for first of two sided figures.

2. Basis

2.1. General layout of DDS thermal items

The DDS thermal items are composed by 18 *physical* heaters and 24 temperature sensors [1]. The general scheme of the distribution and nomenclature is shown in Figure 1, and a scheme only of the EH is presented in Figure 2. Figure 3 shows a global picture of the LTP.

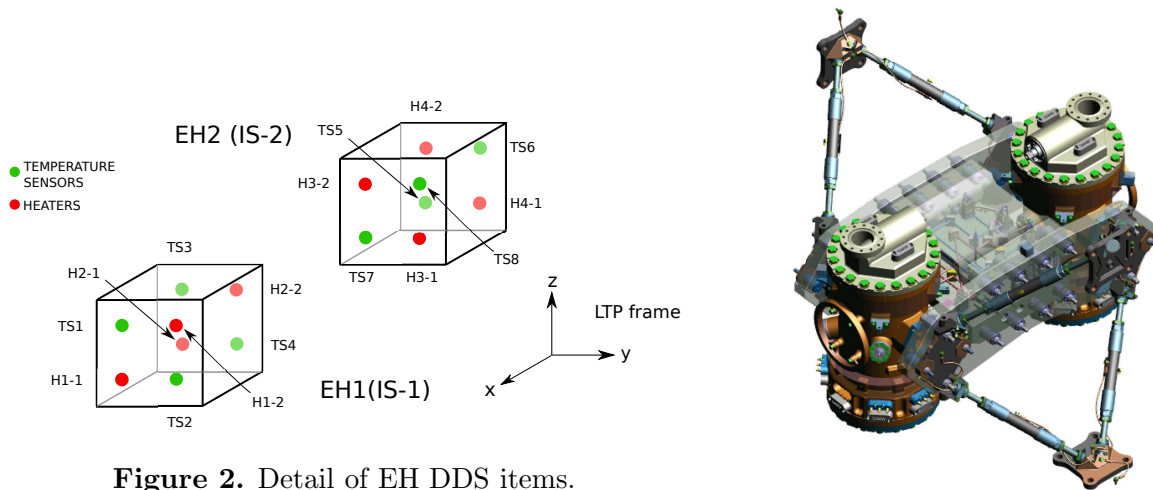


Figure 2. Detail of EH DDS items.

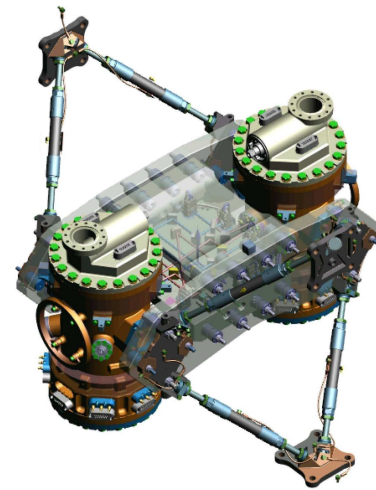


Figure 3. General picture of the LTP.

2.2. EMP thermal calibration description

The Experiment Master Plan (EMP) thermal calibration aims to characterize the consequences of asymmetric temperature fluctuations happening in the LTP. Experiments consist of applying well-defined heat loads at specific points of LTP and observe induced temperature variations at particular points in order to see which are their consequences. Their ultimate goal is to calibrate these effects so that the temperature noise can eventually be subtracted from the IFO readout.

Thermal EMP exercises can be divided into three groups, depending on the main focus of the exercise and the heaters that are being activated:

- (a) Determination of forces and torques on the TMs due to EH heaters activation.
- (b) Determination of IFO phase shifts due to Optical Window (OW) heaters activation.
- (c) Determination of IFO phase shifts due to Suspension Struts (STR) heaters activation.

Dynamic effects from exercises performed at (a) come as a result of the existence of different thermal effects appearing in the EH environment - see Section 2.4-, while experiments from (b) and (c) are aimed to analyze thermoelastic effects caused by heating the OWs and creating stresses on the Optical Bench, respectively, and should not interfere with the TMs dynamics.

The specific input power sequences are described in Table 1 [2, 3]. They are intended to generate enough *disturbance* in specific spots so the IFO can detect their presence. However, they may present side effects that must be also studied, particularly in the dynamics of the TM during exercises (b) and (c), due to the amount of total heat applied.

Table 1. Input signals for each experiment. Experiments from (a) apply heat to pairs of EH heaters from same face of a TM alternatively, while in ones from (b) and (c) simple pulse series are applied to single a heater each time.

Experiment	Power	Period	Duty cycle	Duration
(a) EH	1-80 mW	2000 s	50%	4000 s
(b) OW	0.1-1 W	1000 s	5%	5000 s
(c) STR	0.5-2 W	2500 s	4%	7500 s

2.3. Signal requirements

LPF main noise requirements are given as a spectral density of noise by [5]

$$S_{\Delta a, \text{LPF}}^{1/2}(\omega) \leq 3 \times 10^{-14} \left[1 + \left(\frac{\omega/2\pi}{3 \text{ mHz}} \right)^2 \right] \text{ m s}^{-2} \text{ Hz}^{-1/2} \quad (1)$$

in the band from 1mHz to 30 mHz. Considering that the mass of each TM is 1.96 kg [4], Equation 1 consequent conversion to force requirement is expressed with

$$S_{\Delta F, \text{LPF}}^{1/2}(\omega) \leq 5.9 \times 10^{-14} \left[1 + \left(\frac{\omega/2\pi}{3 \text{ mHz}} \right)^2 \right] \text{ N Hz}^{-1/2} \quad (2)$$

On the other hand, the SNR requirement to detect thermally created signals in the inertial sensor (IS) with the IFO is $SNR \geq 50$ [5], and it is obtained, considering a force signal $F(t)$, as

$$(SNR)^2 = \frac{2}{\pi} \int_{BW} \frac{|\tilde{F}(w)|^2}{S_{\Delta F, \text{LPF}}(w)} dw \quad (3)$$

where $\tilde{F}(w)$ is the Fourier Transform of the force signal $F(t)$.

2.4. Thermal effects

Temperature differences across the TMs environment can produce differential pressures that turn to net forces and torques on the TMs. Three different thermal effects have been identified as mechanisms responsible of these quantities [6]:

2.4.1. Radiation pressure effect It is based on the temperature-dependence of the radiation emitted by a heated surface. The pressure generated is expressed as:

$$P_{\text{rdn}} = \frac{8}{3} \frac{\sigma T^3}{c} \Delta T \text{ Pa} \quad (4)$$

where σ is the Stefan-Boltzmann constant, c is the speed of light, T is the absolute temperature and ΔT is the temperature difference between two surfaces.

2.4.2. Radiometer effect It appears in rarified atmospheres where the particles have a mean free path much longer than the distance between the two surfaces. The consequent pressure is represented here as:

$$P_{\text{rmt}} = \frac{1}{4} \frac{p}{T} \Delta T \text{ Pa} \quad (5)$$

where p stands for the remaining gas static pressure. T and ΔT have same meanings as in Equation 4.

2.4.3. Outgassing effect A third thermal effect with poorly known consequences, the outgassing effect could appear. Models of this effect made so far are not accurate enough, therefore it will not be considered here.

3. Procedure

The procedure can be split in two parts, the first one concerning all the operations related with the data from the thermal model and the following fit that allows to calculate the temperature distribution, and the second one related with the force modelling.

3.1. Thermal model

The thermal model used to simulate the thermal behaviour of the different parts under analysis is the current ESATAN version that can be found at ESTEC. Samples of transfer functions containing the temperature response in a node after applying heat into another can be directly determined by the ESATAN program.

A set of specific thermal nodes concerning the temperature sensor nodes and the nodes of the different electrodes in the EH were selected as representative of the temperature distribution response [7], and their transfer function samples were provided by ESTEC. Data was fitted using LTP Data Analysis Tool software in order to get analytic expressions for each *node to node* relation.

Additionally to these transfer functions, specific thermal behavior for the heaters modelling their thermal resistance was considered also [8], and it was combined with the initial transfer functions so as to get a more approximate model of the case. With the definitive relation, time response of temperature at different points due to the activation of different heaters were directly determined.

Figure 4 shows a group of Bode Plots as an example of the different transfer functions obtained.

3.2. Modelling forces

Considering the geometry of the case and assuming that only the faces containing EH heaters are relevant for the calculation of forces along the X axis, it is possible to express the resulting force with Equation 6.

$$F_X = F_{\text{rdn}} + F_{\text{rmt}} = \frac{8}{3} \frac{\epsilon_{ij} A \sigma T_0^3}{c} \Delta T_{AB} + \frac{1}{4} \frac{Ap}{T_0} \Delta T_{AB} = \left(\frac{8}{3} \frac{\epsilon_{ij} A \sigma T_0^3}{c} + \frac{1}{4} \frac{Ap}{T_0} \right) \Delta T_{AB} \text{ N} \quad (6)$$

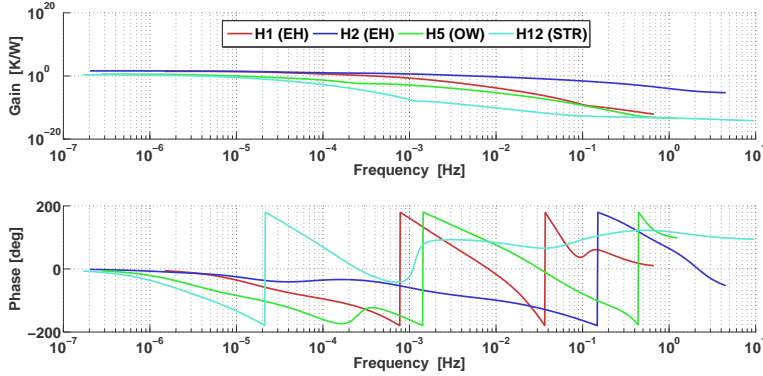


Figure 4. Bode plots of the temperature response at temperature sensor TS3 location (-X face of EH1). The different heaters considered are H1, H2, H5 and H12.

where A is the area where the pressure is applied and ϵ_{ij} is the view factor between two EH-TM surfaces.

Replacing with the nominal values of the case [4] and considering a view factor $\epsilon_{ij} = 0.683$, the resulting temporal *force-temperature* relation states $F_X(t) = 36.4\Delta T(t)$ pN, where $\Delta T(t)$ is the temperature difference between both X inner faces of a single EH at time t .

4. Results

4.1. EH heaters

Figures 5 and 6 present the time response of the temperature gradient and force in X axis with a power input of 10mW. The higher amplitude of the first peak in Figure 6 is created due to the initial *cold* environment in the EH. Therefore, the total force applied will tend to be assymetrical.

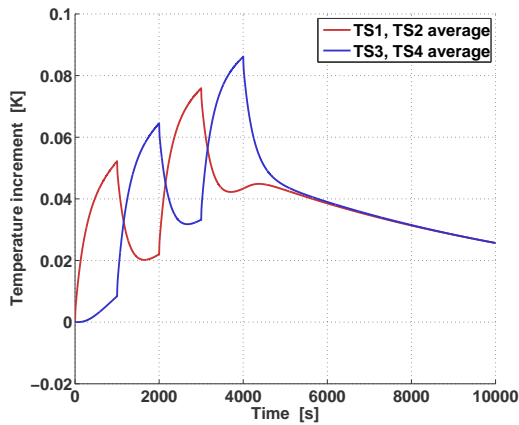


Figure 5. Absolute temperature increment values for each side of TM-1 along exercise (a).

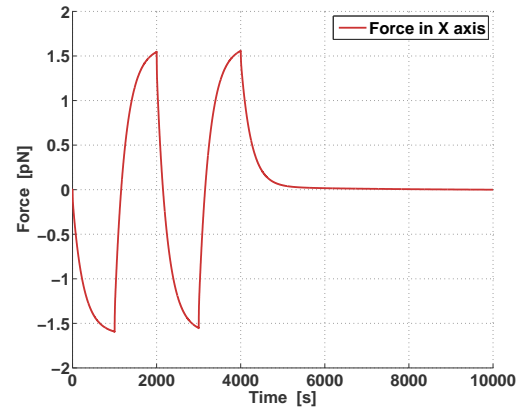


Figure 6. Force in X axis on TM-1 along exercise (a).

The SNR obtained from this exercise is of about 116, considering an integration time of 50,000 seconds, what meets the requirement.

4.2. Side effects on EH

Exercise (b) produces a SNR due to forces in EH of ~ 0.93 when a power of 0.2 W is applied, while exercise (c) gets a SNR of ~ 0.02 with a power of 2 W. In both cases, an integration time of 100,000 seconds was considered.

4.3. Transient times

The transient time length is also of great interest, because it sets the required relaxation time between different exercises and the total length of the experiment. Taking into account that considerable amounts of power are applied in some cases, it should be expected that long periods of time would be required between different exercises.

For example, referring to exercise (a), the time that it takes for the EH to cool back to 10% of the maximum absolute temperature reached is about 22,000 s, while the time that it needs to recover to 10% of maximum differential temperature is about 4,600 s.

However, for the cases of exercises (b) and (c) it is not that clear, as the hottest points are reached far from the EH. Relaxation times of these exercises can easily be a matter of days, although they vary with the distance of the heater to each EH and the total amount of heat applied.

5. Conclusions

Thermal response of the EH thermistors to the activation of the different LTP heaters already analysed. Analysis results so far point to:

- EH heaters activation parameters produce forces on the TM which are 100 or more times the background noise.
- Depending on the applied power, OW heating can be sensed in the EH with SNR around 1.
- STR heating does not cause noticeable effects at TM.

It is important to remark that the current power margins allow a set of possible heat inputs that in some cases could involve quite long relaxation times. In order to assess them appropriately, more detailed analysis of each case should be done, including thermoelastic effects, which are beyond the scope of this paper. Further work is still required, specifically in detailing a more accurate temperature distribution around the TMs, that will be obtained from ESATAN-provided electrode temperatures. This more detailed data will have to be correlated with the EH temperature sensor readouts.

Finally, forces in the Y and Z axes of the EH must, and will be studied, as well as torques generated from the same sources, although their impact is not expected to affect too much. Work is currently underway on these matters.

Acknowledgments

This study has been supported by MICINN-CSIC contract ESP2007-61712. FG also acknowledges a grant from the project *Hibridació d'assignatures d'elevat contingut tecnològic com a prova pilot per als nous plans d'estudis de Grau i Màster de la titulació d'Enginyeria Aeronàutica a l'ETSEIAT*, from Departament de Projectes d'Enginyeria at ETSEIAT-UPC.

References

- [1] G Kahl 2007, *DDS Subsystem Specification*, Report S2-ASD-RS-2004, v4.4.
- [2] M Nofrarias *et al* 2009, *Thermal experiments on board LTP*, Report S2-IEC-TN-3042, v1.1.
- [3] M Nofrarias 2006, *DDS heaters characterisation*, Report S2-IEC-TN-3025, v1.1.
- [4] N Brandt *et al* 2007, *Experiment Performance Budget*, Report S2-ASD-RP-3036, v2.
- [5] S Vitale *et al* 2005, *Science Requirements and Top-Level Architecture Definition for the LISA Technology Package (LTP) on Board LISA Pathfinder(SMART2)*, Report LTPA-UTN-ScRD, Iss3-Rev1.
- [6] M Nofrarias 2007, *Thermal diagnostic in the LISA technology package experiment*, Chapter 2. PhD thesis, Barcelona.
- [7] A Lobo 2010, *LTP thermal response to periodic signals injected by heaters*, Report S2-IEC-TN-3059, v1.
- [8] J Sanjuán 2009, *Development and validation of the thermal diagnostics instrumentation in LISA Pathfinder*, Appendix B. PhD thesis, Barcelona.

Bibliography

- [1] A Franzoso 2007, *LISA Core Assembly Thermal Model Description*, Technical Note S2-CGS-TN-3031.v2.
- [2] J. R. Howell. *A catalog of radiation heat transfer configuration factors*
<http://www.me.utexas.edu/~howell/> <http://www.rssd.esa.int/index.php?project=LISAPATHFINDER>
- [3] J Sanjuán 2009, *Development and validation of the thermal diagnostics instrumentation in LISA Pathfinder*, Appendix B. PhD thesis, Barcelona.